Proc. Natl. Acad. Sci. USA
Vol. 96, pp. 5412–5417, May 1999
Biochemistry

The crystal structure of a multifunctional protein: Phosphoglucose isomerase/autocrine motility factor/neuroleukin

YUH-JU SUN*, CHIA-CHENG CHOU*†, WEI-SHONE CHEN‡, RONG-TSUN WU§, MENGHSIAO MENG¶, AND CHWAN-DENG HSIAO*‖

*Institute of Molecular Biology, Academia Sinica, Taipei, Taiwan 11529, Republic of China; †Graduate Institute of Life Science, National Defense Medical Center, Taipei, Taiwan 11217, Republic of China; ‡Veterans General Hospital, Taipei, Taiwan 11221, Republic of China; §Graduate Institute of Biopharmaceutical Science, National Yang-Ming University, Taipei, Taiwan 11221, Republic of China; and ¶Graduate Institute of Agricultural Biotechnology, National Chung Hsing University, Taichung, Taiwan 40227, Republic of China

Edited by Robert Huber, Max Planck Institute for Biochemistry, Martinsried, Germany, and approved March 20, 1999 (received for review December 21, 1998)

ABSTRACT **Phosphoglucose isomerase (PGI) plays a central role in both the glycolysis and the gluconeogenesis pathways. We present here the complete crystal structure of PGI from *Bacillus stearothermophilus* at 2.3-Å resolution. We show that PGI has cell-motility-stimulating activity on mouse colon cancer cells similar to that of endogenous autocrine motility factor (AMF). PGI can also enhance neurite outgrowth on neuronal progenitor cells similar to that observed for neuroleukin. The results confirm that PGI is neuroleukin and AMF. PGI has an open twisted α/β structural motif consisting of two globular domains and two protruding parts. Based on this substrate-free structure, together with the previously published biological, biochemical, and modeling results, we postulate a possible substrate-binding site that is located within the domains' interface for PGI and AMF. In addition, the structure provides evidence suggesting that the top part of the large domain together with one of the protruding loops might participate in inducing the neurotrophic activity.**

Phosphoglucose isomerase (PGI; EC 5.3.1.9) is a glycolytic enzyme that catalyzes the reversible isomerization of glucose-6-phosphate to fructose-6-phosphate. PGI deficiency in humans leads to nonspherocytic hemolytic disease (1, 2). In addition, the serum activity of PGI has been established as a tumor marker in human cancer patients (3, 4), and elevation in PGI activity is closely correlated with metastasis (5, 6).

Recently, it has been shown that several important proteins, neuroleukin (NLK; refs. 7–9), autocrine motility factor (AMF; refs. 10 and 11), and maturation factor (MF; refs. 11 and 12), are closely related, if not identical, to PGI. Mouse and human NLKs can be aligned with pig muscle PGI without any sequence insertions or deletions. Including conservative substitutions, mouse NLK has 87% and 90% sequence identity with human NLK (8) and pig muscle PGI (7), respectively. The primary structural differences are mostly conservative substitutions that probably reflect species and organ specificities.

NLK is a neurotrophic growth factor. It promotes motor neuron regeneration *in vivo*, fosters the survival of peripheral and central neurons *in vitro*, and affects B cell Ig synthesis (13, 14). Interestingly, the dimeric form of NLK carries out its isomerase activity, whereas the monomeric form of the protein is responsible for the neurotrophic activity (9). In the presence of monomeric PGI, neuroblastoma cells have enhanced neurite extension and a reduced proliferation rate (9). These results suggest that PGI has a growth factor-like activity and that PGI is potentially related to NLK.

AMF (10, 15–17) represents a class of cytokines: a group of proteins that control cell growth and differentiation in embryogenesis, immunity, and inflammation (18). They are produced locally and act in an autocrine or paracrine manner. AMF was identified originally by its ability to induce directed random migration of cells. It has since been implicated in stimulating motility during cell invasion and metastasis (10, 15).

AMF regulates growth and motility by a receptor-mediated signaling pathway. On signal transduction, AMF binds to a cell surface glycoprotein of 78 kDa (19–21), implying that AMF is the natural ligand of the 78-kDa glycoprotein (17). AMF secreted by Gc-4 PF murine fibrosarcoma cells (10) has PGI activity, whereas rabbit heart PGI can stimulate mouse fibrosarcoma cell motility similar to that of endogenous AMF. More importantly, two specific PGI inhibitors, 6-phosphogluconic acid and erythrose 4-phosphate, can inhibit the isomerase activity of PGI (22) and abolish the AMF-induced cell motility (10). The results support the notion that murine AMF is a PGI.

MF mediates the differentiation of human myeloid leukemic HL-60 cells to terminal monocytic cells (12). Interestingly, the purified MF has been shown to have PGI enzymatic activity, and the purified PGI also has the differentiation property for leukemia cells ascribed to the MF (12). The amino acid sequence of a tryptic and the enzyme cleavage sites of MF is 100% homologous to both NLK and PGI (12).

Although studies on PGI have proved a close enzymatic relationship with NLK, AMF, and MF, nothing is known about the structural basis of these activities. Previously, we have reported the expression of two *Bacillus stearothermophilus* PGIs (PGI-A and PGI-B) in *Escherichia coli* (23). In this study, we show that *Bacillus* PGI stimulates the cell motility of CT-26 mouse colon tumor cells and enhances the neurite outgrowth on neuronal progenitor cells. We also present the crystal structure of PGI-B at 2.3-Å resolution by x-ray diffraction.

MATERIALS AND METHODS

Crystallization and Structure Determination. The isolation, purification, and crystallization of PGI have been reported (23). Crystals were grown by the hanging-drop vapor-diffusion method from solutions containing ammonium phosphate as the precipitant. The crystals belong to space group I222 with the cell dimensions $a = 75.1$ Å, $b = 93.7$ Å, and $c = 171.9$ Å; one molecule per asymmetric unit. After an extensive search, two useful derivatives, $KAu(CN)_2$ and HgI_2, were obtained by soaking native

The publication costs of this article were defrayed in part by page charge payment. This article must therefore be hereby marked "*advertisement*" in accordance with 18 U.S.C. §1734 solely to indicate this fact.

PNAS is available online at www.pnas.org.

This paper was submitted directly (Track II) to the *Proceedings* office.
Abbreviations: PGI, phosphoglucose isomerase; AMF, autocrine motility factor; NLK, neuroleukin; MF, maturation factor; EGF, epidermal growth factor.
Data deposition: The atomic coordinates have been deposited in the Protein Data Bank, Biology Department, Brookhaven National Laboratory, Upton, NY 11973 (PDB ID code 2PGI).
‖To whom reprint requests should be addressed. e-mbhsiao@ccvax.sinica.edu.tw.

crystals in heavy-atom solutions. All data used for structure determination were collected on a Rigaku (Tokyo) R-Axis II Imaging Plate mounted on a Rigaku RU300 rotating-anode. The data were indexed, integrated, and scaled by using DENZO and SCALEPACK (ref. 24; Table 1).

The heavy-atom positions were located by difference Patterson techniques and refined by using the CCP4 (Collaborative Computational Project, November 4, 1994) implementation of MLPHARE (24). The ISIR-ISAS program (25) was used to generate the initial MIRAS (multiple isomorphous replacement including anomalous scattering) phases at 3.5-Å resolution followed by phase extension to 3.0 Å. The resulting electron-density map showed a molecular boundary indicative of a two-domain structure and evidence of several α-helices and β-sheet strands in both domains. The initial MIRAS phases were improved further by the program DM (26) by using a combination of solvent flattening, histogram mapping, and Sayre's equation (skeletonization was not included in this calculation). The MIRAS map showed continuous electron density with well defined side chains for almost the entire molecule. The initial model, which contained 440 residues and 3,508 nonhydrogen atoms, resulted in a conventional R factor of 39.8% from 8 Å to 2.8 Å with $2\sigma(F)$.

The model was refined against data between 8.0 Å and 2.3 Å by simulated annealing and positional refinement by using the program X-PLOR 3.1 (27). Individual atoms were assigned isotropic B factors, which were refined during the latter stages of the refinement. Fig. 1 shows a sample final omitted ($2F_o - F_c$) map. The final model contains 3,699 nonhydrogen atoms, including 184 oxygen atoms from water molecules. The first and the last two amino acid residues are presumably disordered in the crystal structure. The R factor is 18.5% for all $2\sigma(F)$ data between 8.0-Å and 2.3-Å resolution. By using a 10% reflection test set (2,319 reflections), the R_{free}-value (28) is 25.8%. The model has good stereochemistry with rms deviations in bond lengths and angles of 0.012 Å and 1.348°, respectively. Analysis of the Ramachandran plot (29) shows no violations of accepted backbone torsion angles. Atomic coordinates have been deposited with the Protein Data Bank (ref. 30; ID code 2PGI).

Cell-Motility Assay. Cell motility of mouse CT-26 cells was measured by the method described by Lin *et al.* (31) with minor modifications. Polyvinylpyrrolidone-free polycarbonate filters (Nuclepore; 8-μm pore size) were soaked in 0.5 M acetic acid overnight. The filters were washed with distilled water and coated with 50 μl of matrigel for 2 h. Cells were placed on the top of a Boyden chamber at a cell dose of 5×10^4 per 200 μl in MEM with 10% FBS. Incubation was carried out at 37°C for 8 h. The filters were removed and fixed in 4% paraformaldehyde for 15 min at room temperature. Cells on the upper filter surface were removed carefully with a cotton swab. The filters were stained with hematoxylin for 40 min. Cells on the lower filter surface were counted under a light microscope.

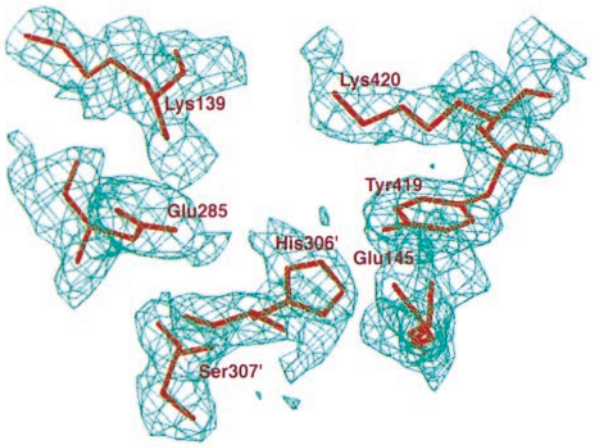

FIG. 1. The omitted $2F_o - F_c$ electron density map of PGI from regions of the proposed substrate-binding site. The map was calculated by omitting Lys-139, Glu-285, His-306, and Lys-420 from the x-ray model. Simulated-annealing refinement was performed with a 3-Å spherical shell of fixed atoms surrounding the omitted regions and was contoured at the 1.0-σ level. Residues His-306′ and Ser-307′ belong to the symmetry-related subunit in a dimer.

Neurite-Outgrowth Assay. Morphological responses to PGI of rat epidermal growth factor (EGF)-responsive neuronal embryonic progenitor cells (32, 33) were assayed. The serum-free

Table 1. X-ray crystallography data

Statistic	Data set		
	Native	kAu $(CN)_2$	HgI_2
Data collection and phasing			
Resolution (Å)	2.3	2.5	2.5
Reflection, unique/total	24,024/104,060	20,666/120,404	20,699/117,909
Data completeness (%); overall (final shell)	93.9 (83.4)	97.2 (96.2)	96.7 (92.3)
Heavy-atom concentration	—	1 mM	20%
Soaking time, days	—	2	2
R_{merge}* (%) (final shell)	7.0 (36.2)	7.1 (34.3)	10.0 (41.8)
R_{iso}† (%)	—	12	11
Heavy-atom binding site	—	1	2
R_{cullis}‡, 15–3.0 Å	—	0.70	0.74
Phasing power§, centric/acentric	—	1.11/1.05	0.91/1.13
Refinement			
Resolution (Å)	8–2.3		
R-factor (%)	18.5		
R_{free} (%)	25.8		
Observation $F > 2\sigma$ (F)	23,447		
Total number of protein atoms	3,515		
Total number of water molecules	184		
rmsd bond lengths (Å)	0.012		
rmsd bond angles (degree)	1.348		

rmsd, root-mean-square deviation.
*$R_{merge} = \Sigma\Sigma_j|I_j - \langle I\rangle|/\Sigma\langle I\rangle$.
†$R_{iso} = \Sigma||F_{ph}|-|F_p||/\Sigma|F_p|$.
‡R_{cullis} = lack of closure/isomorphous difference.
§Phasing power = F_H/lack of closure.

culture medium was made up of an equal mixture of DMEM and F-12 nutrient (GIBCO), supplemented with insulin (25 μg/ml), transferrin (50 μg/ml), progesterone (20 nM), putrescine (100 μM), and selenium chloride (30 nM). Brains were removed from 17-day-old Sprague–Dawley rat embryos and dissociated mechanically with a fire-polished Pasteur pipette. After culturing for 4–5 days in the serum-free medium supplemented with 20 ng/ml EGF, the primary EGF-responsive embryonic neuronal progenitor cells were dissociated into single cells. The cells were then transferred to 96-well plates and cultivated in the serum-free medium supplemented with EGF (10 ng/ml) in the presence or absence of PGI.

RESULTS AND DISCUSSION

The Overall Structure. The overall folding of a PGI monomer is shown in Fig. 2. The molecule is divided clearly into two globular domains (designated as large and small domains) and an "arm-like" C-terminal tail. Both the large and the small domain have a central core of a β-pleated sheet flanked by α-helices to form a typical α/β folding motif. The large domain also contains a protruding loop region diametrical to the C-terminal tail. Therefore, the overall shape of the subunit is somewhat ellipsoidal with an "arm-like" structure on each side.

The secondary structure of the large domain containing the N-terminal of the protein is built from two separate peptide segments (residues 2–34 and 236–403). This domain has two antiparallel strands (β10 and β11) that are placed roughly perpendicularly to a central five-stranded β-sheet (β1, β7, β8, β9, and β12). Consequently, β10 and β11 form an arm-like protruding loop. There are two (α14 and α15) and three α-helices (α12, α13, and α16) on either side of the central five-stranded β-sheet. From the α3 helix, the chain progresses to form the entire supersecondary structure of the small domain.

The small domain encompasses residues 56–217. It has also a five-stranded β-sheet (β2, β3, β4, β5, and β6) at the core. The β-sheet is sandwiched by three helices on one side (α4, α5, and α10) and four α-helices on the other (α6, α7, α8, and α9), forming a typical open twisted α/β folding structure. Lastly, the C-terminal 32 amino acids (residues 414–445) of the protein fold into two consecutive helices (α17 and α18) linked by a short turn.

Because the large domain is built from two separate peptide segments, it is connected to the small domain by two helices, α3 (residues 43–51) and α11 (residues 220–236). Despite the discontinuity in the large domain, the sheet topologies are similar in both domains. All the β-strands in both domains are parallel, except for the β1 and the protruding loop (β10 and β11) in the large domain, which are antiparallel. The β-strands of the small domain point toward the C-terminal tail, whereas those from the large domain are oriented antiparallel to those of the small domain and point toward the protruding loop region. The arrangement of the small globular domain and the C-terminal tail results in a slight cleft wherein the substrate might be bound.

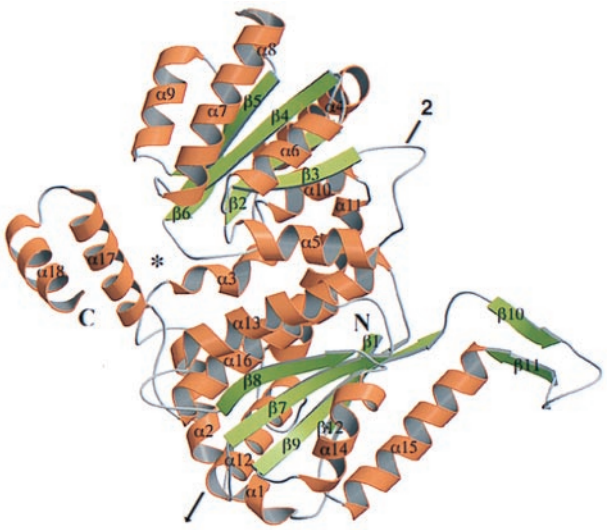

FIG. 2. A ribbon drawing (64, 65) of the PGI monomer with the small domain on the top, the large domain on the bottom, and the C-terminal domain on the left. α-Helices are colored gold and labeled α1–α18. β-Strands are in green and labeled β1–β12. The proposed substrate-binding site is indicated by an asterisk. The crystallographic 2-fold axis that runs through the dimer is shown by an arrow.

The functional form of the PGI is a dimer. However, there is only a single subunit in the crystallographic asymmetric unit. The dimer is globular in shape with dimensions of $\approx$78 Å $\times$ 75 Å $\times$ 50 Å. The subunits associate in an arm-to-arm hug fashion with intimate contacts and form a hydrophilic channel that coincides with the crystallographic 2-fold axis that runs through the dimer as indicated by an arrow in Fig. 2. Most of the monomer–monomer interactions are formed among helices and loops, because the β-sheets are in the cores and sandwiched by helices. Intersubunit contacts are constituted mainly among β2, α6, α7, α9, α13, α14, α15, α17, α18, and the loop regions. The dimer is stabilized by a total of 76 intermolecular hydrogen bonds ($\leq$3.5 Å) as well as van der Waals interactions.

Structure Comparison with Other Isomerases. A crystal structure of pig muscle PGI was previously determined at 3.5-Å resolution (34, 35). However, because of the resolution limit and the lack of sequence information, the C_α backbone of pig PGI could not be traced throughout the whole structure and not all the amino acid side chains could be defined. In that model, 85% of the C_α atoms were built, and both the N and the C termini were assigned tentatively. Pig PGI is a dimeric enzyme and reportedly has an α/β folding motif. Each subunit consists of a large and a small domain. The large domain contains a six-stranded parallel β-sheet surrounded by α-helices. The small domain contains a four-stranded parallel β-structure surrounded by helices and an irregularly folded chain. Similar to the PGI structure of *B. stearothermophilus*, the subunit is somewhat ellipsoidal, and a slight cleft is observed between the two domains.

It is interesting to compare the three-dimensional structure of PGI with the structures of triose phosphate isomerase (TPI; ref. 36) and D-xylose isomerase (37–39). TPI catalyses the interconversion between D-glyceraldehyde-3-phosphate and dihydroxyacetone phosphate (36), whereas xylose isomerase is involved in the transposition of xylose to xylulose. A "hydride-transfer" mechanism has been proposed for xylose isomerase (40–43). However, biological and biochemical studies (38, 44) suggest that both PGI and TPI use instead a "proton-transfer" mechanism. The proton-transfer mechanism involves the formation of an *cis*-enediol intermediate by transferring a proton between C1 and C2 of the sugar ring. Although different mechanisms pertain to the triose phosphate and the xylose isomerization reactions, both enzymes form the typical eight-stranded α/β barrel (TIM barrel) motif structure. In contrast, the PGI model from *B. stearothermophilus* has an open twisted α/β structure.

PGI Stimulates Cell Motility. Rabbit PGI has been shown to induce directed random migration of tumor cells and implicated as an AMF (10, 17). Results from amino acid sequencing analysis and immunological cross-reactivity also suggest that mouse AMF is identical or closely related to PGI/NLK. Whether *B. stearothermophilus* PGI has AMF activity can be addressed directly by observing its migratory-stimulation activity in cell-motility assays. Purified PGI from *B. stearothermophilus* stimulates CT-26 mouse colon cancer cell motility in a dose-dependent fashion and exerts maximal stimulating activity between 10 pg/ml and 100 pg/ml. Fig. 3 is a pictorial demonstration of the motility assay and the stimulatory effect on CT-26 cells in the absence (Fig. 3*A*) or presence (Fig. 3 *B* and *C*) of PGI. The results are consistent with those observed by Watanabe *et al.* (10).

Identification of a Putative Substrate-Binding Site of PGI/AMF. After finding that *Bacillus* PGI is functionally equivalent to

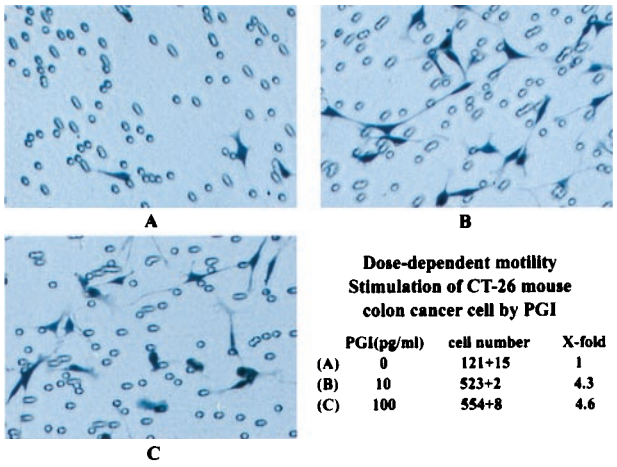

FIG. 3. Dose-dependent motility stimulation of CT-26 mouse colon cancer cells by purified *B. stearothermophilus* PGI. CT-26 cells were plated in culture medium in the absence or various concentrations of PGI. Representative photomicrographs of cells plated in the absence (*A*) or presence of 10 pg/ml (*B*) or 100 pg/ml (*C*) PGI are shown.

AMF, the next obvious issue is to locate the substrate-binding site on PGI/AMF. Because PGI and AMF share the same substrate and inhibitors (i.e., carbohydrate phosphates; ref. 10), the implicated binding site should also be the same for both proteins.

The genes coding for PGI have been isolated from a variety of sources ranging from bacteria to mammals (35, 45–47). Two regions of conserved amino acids, [LIVM]-G-G-R-[FY]-S-[LIVM]-x-[ST]-A-[LIVM]-G and [FY]-D-Q-x-G-V-E-x-x-K, have been identified (Fig. 4) and are documented as signature patterns for the PGI (48) superfamily. Members of this superfamily include *B. stearothermophilus* PGI, pig muscle PGI, human PGI/NLK/AMF, and mouse PGI/NLK. Residues inside the square brackets above represent the evolutionarily conserved residues. The corresponding regions are residues 198–210 from the small domain and 411–420 from the large domain in *B. stearothermophilus* PGI. Interestingly, these two conserved regions are located within the slight cleft area in our model. Therefore, it is reasonable to propose that all PGIs have the same evolutionary origin and employ the same catalytic mechanism.

A base-catalyzed mechanism has been proposed for the interconversion of aldose and ketose via a *cis*-enediol intermediate (49, 50). Based on chemical modification and affinity-labeling experiments, histidine (51), lysine (52), glutamate (53), and arginine (54) residues have been postulated to be involved in the catalytic process. Results from site-directed mutagenesis and kinetic studies (47) also suggested that Lys-139, Arg-202, Lys-289, and Lys-420 are located in the active site of the *B. stearothermophilus* PGI. As determined by the crystallographic studies of pig (34, 35) and rabbit PGIs (2), the active site is situated in a cleft between the large and small domains of the monomer and is formed by the association of the two subunits. Their results showed that histidine and glutamate residues might be situated in the active site of PGI. Kugler *et al.* (2) also pointed out that the histidine residue involved in enzymatic reaction is from the other subunit. Moreover, the involvement of lysine and arginine residues in the binding of phosphate groups by various enzymes, such as 6-phosphofructo-2-kinase (55, 56), glycogen phosphorylase b (57), maltodextrin phosphorylase (58), protein tyrosine phosphatase 1B (59), and protein phosphatase 1 (60), have been well studied.

Based on the substrate-free PGI structure described in this work, together with the aforementioned biological and biochemical results, we carried out molecular-modeling studies. A possible binding-site geometry that may exist in a PGI-substrate (glucose-6-phosphate) complex was generated by minimizing the distance and neutralizing the opposite charges between the enzyme and the target substrate. A speculative model showing how glucose-6-phosphate could be docked into the putative PGI substrate-binding site is presented in Fig. 5. The possible substrate-binding site of PGI is a deep binding pocket located between the large domain, the small domain, and the C-terminal tail.

The isomerization reaction is initiated by a ring-opening step, followed by a proton-transfer process and a ring-closure procedure. In this postulated complex model, Arg-202, Glu-285, and

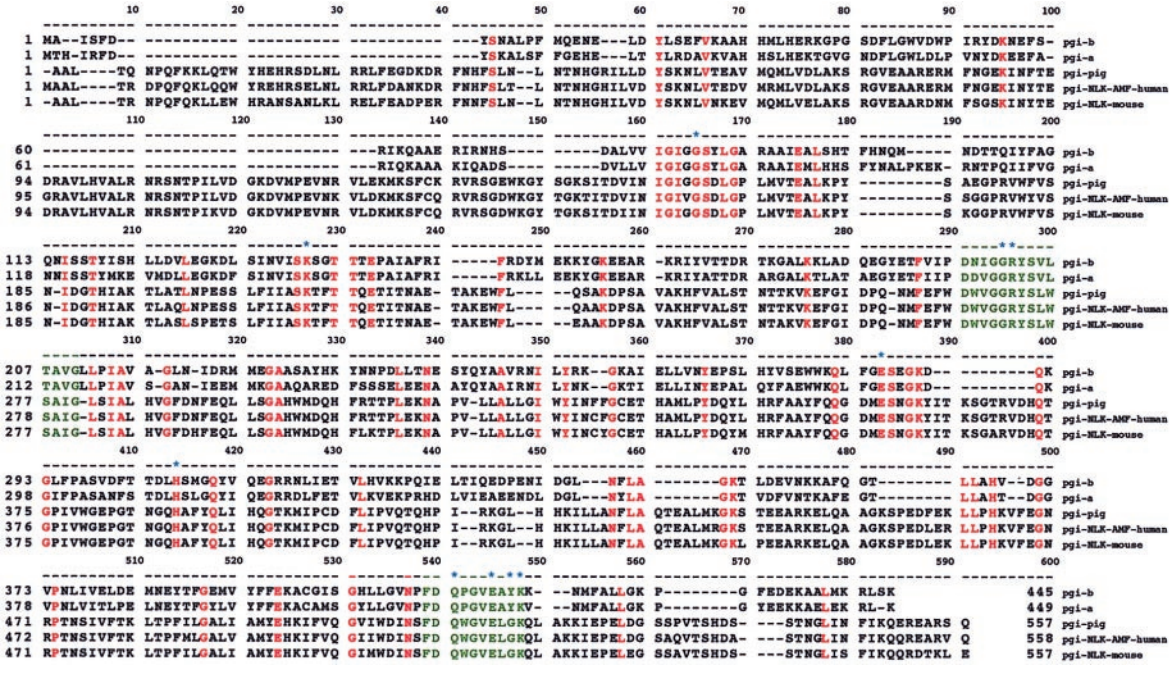

FIG. 4. Multiple sequence alignment of the PGI superfamily. Amino acid sequences of *Bacillus* PGI-B, *Bacillus* PGI-A, and PGI from pig, human, and mouse were aligned. Residues that are identical among all five sequences are highlighted in red. Positions of deletions are indicated by dashes. Two signature patterns ([LIVM]-G-G-R-[FY]-S-[LIVM]-x-[ST]-A-[LIVM]-G and [FY]-D-Q-x-G-V-E-x-x-K) of the PGI superfamily are colored in green. Amino acids that form the putative substrate-binding sites are denoted by asterisks.

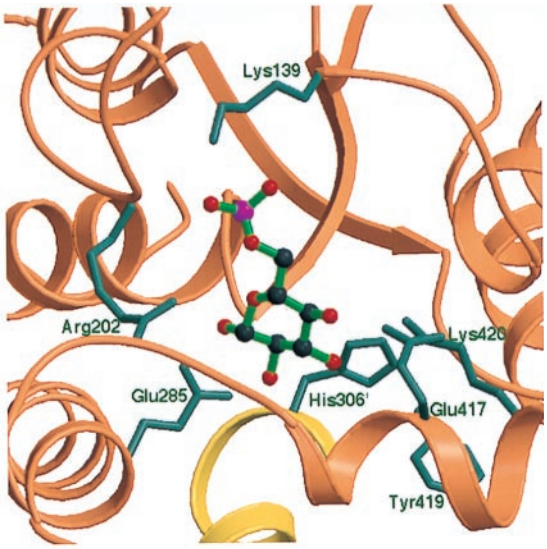

FIG. 5. A ribbon drawing (64, 65) showing the proposed substrate-binding site as determined by the substrate-free PGI structure. The glucose-6-phosphate is represented by balls and sticks and is colored in red (oxygen), deep blue (carbon) and magenta (phosphorus). The residues potentially involved in the enzymatic reaction are labeled by name.

His-306 participate in the catalytic process. Lys-139 forms three salt bridges with the phosphate group to stabilize the substrate. Glu-417, Tyr-419, and Lys-420 interact with the hydroxyl groups of C3 and C4 of the substrate via hydrogen bonds. Glu-285 and His-306 are the two most likely candidates for the base-catalytic and proton-transfer steps in the phosphoglucose isomerization. It is interesting to point out that the His-306 positioned in this possible binding site is from the other subunit of the dimer. This positioning may explain why the active form of the isomerase is a dimer. All these important residues, except Tyr-419, are conserved in the multiple sequence alignment (Fig. 4). Certainly, crystal structures of the substrate/inhibitor-enzyme complex definitely are needed before the role of these residues can be defined explicitly.

PGI Enhanced Neurite Outgrowth. Many studies (7, 8, 10, 61) have shown that PGI has a close functional relationship with

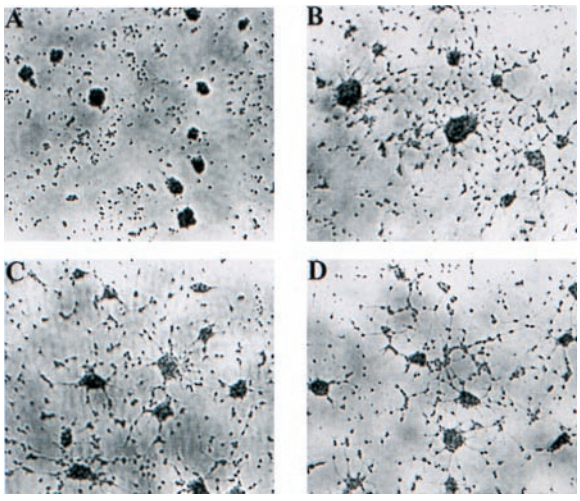

FIG. 6. Morphological response of rat EGF-responsive neuronal embryonic progenitor cells promoted by PGI. (*A*) After 4 days of cultivation in the absence of PGI, the neuronal progenitor cells formed a single sphere of undifferentiated morphology, compared with a differentiated morphology of neurite outgrowth treated with 2 ng/ml PGI (*B*), 20 ng/ml PGI (*C*), and 200 ng/ml PGI (*D*).

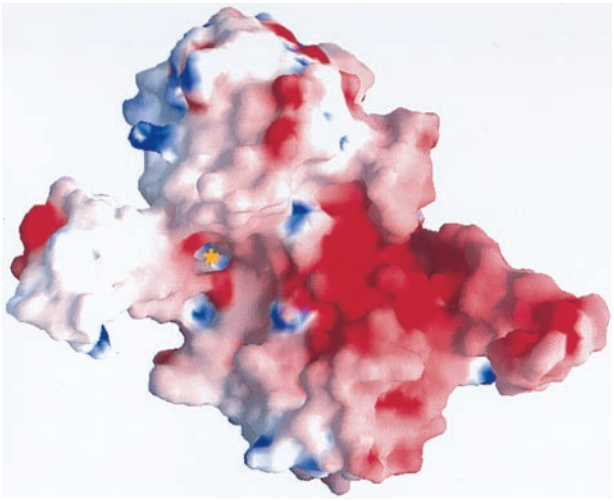

FIG. 7. Electrostatic surface potential on the PGI molecule displayed with the program GRASP (63). Negative potentials (<10 kT) are colored in deep red, and positive potentials (>10 kT) are colored in deep blue. The neutral surface potential regions are depicted in white. The orientation of the molecule is the same as in Fig. 2.

NLK. Three different hypotheses were raised by Gurney (as described in ref. 8) to explain the potential relationship between PGI and NLK: (*i*) the enzymatic activity of PGI may account for the biological response to NLK; (*ii*) PGI may act as a carbohydrate-binding rather than receptor-binding ligand to trigger the biological response to NLK; and (*iii*) either PGI or a processed version of it may be a ligand for a cellular receptor.

To verify that PGI from *B. stearothermophilus* has neurotrophic activity, we examined the morphological response to PGI administration by using rat EGF-responsive neuronal embryonic progenitor cells (32, 33). Compared with controls (Fig. 6*A*), the neurite extensions in these neuronal progenitor cells were significantly greater in number and longer in length when treated with PGI (Fig. 6 *B–D*). The results are consistent with the neurotrophic activities observed by Gurney *et al.* (62) and Mizrachi (9) and confirmed that PGI is NLK.

To identify the regions on PGI that are responsible for NLK activity, we carried out a molecular-surface study on our PGI model. Fig. 7 shows the electrostatic surface potential of the *B. stearothermophilus* PGI monomer displayed by the program GRASP (63). The negatively charged surface (potential < 10 kT) is displayed in deep red, whereas the positively charged surface (potential > 10 kT) is in deep blue. The surface potential of the small domain and the C-terminal region is more neutral and is depicted mostly in white. We have proposed in the last section that the substrate-binding site for PGI/AMF is most likely seated in the junction where the large domain, small domain, and the C-terminal tail come together. In contrast, a strong acidic region is found on the top half of the large domain and the protruding loop (residues 329–352). These distinctive surface-potential regions may be responsible for the NLK activity of PGI. Moreover, Mizrachi (9) reported that a synthetic peptide covering residues 401–421 of the rabbit NLK has cell proliferative activity. In our PGI model, the corresponding residues are 319–339 and located in β10 and the protruding loop. We tentatively proposed that the top part of the large domain and the protruding loop may play another biological function, such as the neurotrophic activity. However, these speculations need to be confirmed by further neurobiological and biochemical study.

CONCLUSIONS

In the present study, we determined the three-dimensional structure of PGI from *B. stearothermophilus* at 2.3-Å resolution by x-ray crystallography. We also demonstrated by cell-migratory stimulation and neurotrophic-activity experiments that PGI has

AMF and NLK activities. A putative substrate-binding site is proposed for further investigation. Our x-ray studies implicate several residues as important in the catalytic reaction. In addition, the structure provides evidence to suggest that the top part of the large domain and the protruding loop may participate in inducing neurotrophic activity for PGI/NLK. However, many questions, such as how PGI exerts its effect on nerve cells; how PGI performs its cell-motility activity; and how PGI switches its enzymatic and biological functions, remain unanswered. The complete high-resolution structure of PGI presented here offers a starting point for further crystallographic, biochemical, genetic, and neurobiological studies of PGI/NLK/AMF. The structure also provides a framework for understanding the structure of other PGI/NLK/AMFs from the same superfamily.

We are grateful to Dr. M. F. Tam of the Institute of Molecular Biology, Academia Sinica for helpful discussions. This work was supported in part by National Science Council Grant NSC87-2311-B-001-025-B21 (to C.-D.H.), Republic of China.

1. Welch, S. G. (1971) *Hum. Hered.* **21,** 467–477.
2. Kugler, W., Breme, K., Laspe, P., Muirhead, H., Davies, C., Winkler, H., Schroter, W. & Lakomek, M. (1998) *Hum. Genet.* **103,** 450–454.
3. Baumann, M., Kappl, A., Lang, T., Brand, K., Siegfried, W. & Paterok, E. (1990) *Cancer Invest.* **8,** 351–356.
4. Baumgart, E., Fahimi, H. D., Stich, A. & Volkl, A. (1996) *J. Biol. Chem.* **271,** 3846–3855.
5. Tor, J., Segura, R. M., Pascual, C., Vilaseca, J., Guarner, M. L. & Schwartz, S. (1981) *Med. Clin. (Barc.)* **77,** 236–239.
6. Tor, J., Pascual, C., Segura, R. M., Vilaseca, J. & Schwartz, S. (1982) *Rev. Clin. Esp.* **164,** 15–18.
7. Chaput, M., Claes, V., Portetelle, D., Cludts, I., Cravador, A., Burny, A., Gras, H. & Tartar, A. (1988) *Nature (London)* **332,** 454–455.
8. Faik, P., Walker, J. I., Redmill, A. A. & Morgan, M. J. (1988) *Nature (London)* **332,** 455–457.
9. Mizrachi, Y. (1989) *J. Neurosci. Res.* **23,** 217–224.
10. Watanabe, H., Takehana, K., Date, M., Shinozaki, T. & Raz, A. (1996) *Cancer Res.* **56,** 2960–2963.
11. Niinaka, Y., Paku, S., Haga, A., Watanabe, H. & Raz, A. (1998) *Cancer Res.* **58,** 2667–2674.
12. Xu, W., Seiter, K., Feldman, E., Ahmed, T. & Chiao, J. W. (1996) *Blood* **87,** 4502–4506.
13. Gurney, M. E., Apatoff, B. R., Spear, G. T., Baumel, M. J., Antel, J. P., Bania, M. B. & Reder, A. T. (1986) *Science* **234,** 574–581.
14. Gurney, M. E. (1987) *Immunol. Rev.* **100,** 203–223.
15. Liotta, L. A., Mandler, R., Murano, G., Katz, D. A., Gordon, R. K., Chiang, P. K. & Schiffmann, E. (1986) *Proc. Natl. Acad. Sci. USA* **83,** 3302–3306.
16. Nabi, I. R., Watanabe, H. & Raz, A. (1990) *Cancer Res.* **50,** 409–414.
17. Watanabe, H., Carmi, P., Hogan, V., Raz, T., Silletti, S., Nabi, I. R. & Raz, A. (1991) *J. Biol. Chem.* **266,** 13442–13448.
18. Thomas, H. & Balkwill, F. R. (1991) *Pharmacol. Ther.* **52,** 307–330.
19. Nabi, I. R., Watanabe, H., Silletti, S. & Raz, A. (1991) *Experientia Suppl.* **59,** 163–177.
20. Nabi, I. R., Watanabe, H. & Raz, A. (1992) *Cancer Metastasis Rev.* **11,** 5–20.
21. Silletti, S., Yao, J. P., Pienta, K. J. & Raz, A. (1995) *Int. J. Cancer* **63,** 100–105.
22. Gracy, R. W. & Tilley, B. E. (1975) *Methods Enzymol.* **41,** 392–400.
23. Hsiao, C. D., Chou, C. C., Hsiao, Y. Y., Sun, Y. J. & Meng, M. (1997) *J. Struct. Biol.* **120,** 196–200.
24. Otwinowski, Z. (1993) in *Proceedings of the CCP4 Study Weekend*, eds. Sawyer, L., Isaacs, N. & Bailey, S. (Sci. Eng. Res. Counc., Warrington, UK), pp. 56–62.
25. Wang, B.-C. (1985) *Methods Enzymol.* **115,** 90–112.
26. Cowtan, K. D. (1996) *Acta Crystallogr. D* **52,** 43–48.
27. Brunger, A. T. (1992) X-PLOR 3.1, A System for Crystallography and NMR (Yale Univ., New Haven, CT).
28. Brunger, A. T. (1992) *Nature (London)* **355,** 472–475.
29. Ramakrishnan, C. & Ramachandran, G. N. (1965) *Biophys. J.* **5,** 909–933.
30. Bernstein, F. C., Koetzle, T. F., Williams, G. J. B., Meyer, E. F., Jr., Brice, M. D., Rodgers, J. R., Kennard, O., Shimanouchi, T. & Tsaumi, M. (1977) *J. Mol. Biol.* **112,** 535–542.
31. Lin, M. T., Wei, S. J. & Wing, L. Y. (1992) *Mol. Cell. Endocrinol.* **84,** 47–54.
32. Reynolds, B. A., Tetzlaff, W. & Weiss, S. (1992) *J. Neurosci.* **12,** 4565–4574.
33. Reynolds, B. A. & Weiss, S. (1992) *Science* **255,** 1707–1710.
34. Shaw, P. J. & Muirhead, H. (1977) *J. Mol. Biol.* **109,** 475–485.
35. Achari, A., Marshall, S. E., Muirhead, H., Palmieri, R. H. & Noltmann, E. A. (1981) *Philos. Trans. R. Soc. London B* **293,** 145–157.
36. Banner, D. W., Bloomer, A. C., Petsko, G. A., Phillips, D. C., Pogson, C. I., Wilson, I. A., Corran, P. H., Furth, A. J., Milman, J. D., Offord, R. E., *et al*. (1975) *Nature (London)* **255,** 609–614.
37. Allen, K. N., Lavie, A., Glasfeld, A., Tanada, T. N., Gerrity, D. P., Carlson, S. C., Farber, G. K., Petsko, G. A. & Ringe, D. (1994) *Biochemistry* **33,** 1488–1494.
38. Lavie, A., Allen, K. N., Petsko, G. A. & Ringe, D. (1994) *Biochemistry* **33,** 5469–5480.
39. Allen, K. N., Lavie, A., Petsko, G. A. & Ringe, D. (1995) *Biochemistry* **34,** 3742–3749.
40. Farber, G. K., Glasfeld, A., Tiraby, G., Ringe, D. & Petsko, G. A. (1989) *Biochemistry* **28,** 7289–7297.
41. Lee, C. Y., Bagdasarian, M., Meng, M. H. & Zeikus, J. G. (1990) *J. Biol. Chem.* **265,** 19082–19090.
42. Collyer, C. A., Henrick, K. & Blow, D. M. (1990) *J. Mol. Biol.* **212,** 211–235.
43. Collyer, C. A. & Blow, D. M. (1990) *Proc. Natl. Acad. Sci. USA* **87,** 1362–1366.
44. Albery, W. J. & Knowles, J. R. (1976) *Biochemistry* **15,** 5627–5631.
45. Mo, Y., Young, C. D. & Gracy, R. W. (1975) *J. Biol. Chem.* **250,** 6747–6755.
46. Muramatsu, N. & Noso, Y. (1971) *Arch. Biochem. Biophys.* **144,** 245–252.
47. Meng, M., Chen, Y.-T., Hsiao, Y.-Y., Itoh, Y. & Bagdasarian, M. (1998) *Eur. J. Biochem.* **257,** 500–505.
48. Bairoch, A., Bucher, P. & Hofmann, K. (1996) *Nucleic Acids Res.* **24,** 189–196.
49. Dyson, J. E. & Noltmann, E. A. (1968) *J. Biol. Chem.* **243,** 1401–1414.
50. Schray, K. J., Benkovic, S. J., Benkovic, P. A. & Rose, I. A. (1973) *J. Biol. Chem.* **248,** 2219–2224.
51. Gibson, D. R., Gracy, R. W. & Hartman, F. C. (1980) *J. Biol. Chem.* **255,** 9369–9374.
52. Schnackerz, K. D. & Noltmann, E. A. (1971) *Biochemistry* **10,** 4837–4843.
53. O'Connell, E. L. & Rose, I. A. (1973) *J. Biol. Chem.* **248,** 2225–2231.
54. Riordan, J. F., McElvany, K. D. & Borders, C. L., Jr. (1977) *Science* **195,** 884–886.
55. Li, L., Lin, K., Kurland, I. J., Correia, J. J. & Pilkis, S. J. (1992) *J. Biol. Chem.* **267,** 4386–4393.
56. Tsujikawa, T., Watanabe, F. & Uyeda, K. (1995) *Biochemistry* **34,** 6389–6393.
57. Lorek, A., Wilson, K. S., Sansom, M. S., Stuart, D. I., Stura, E. A., Jenkins, J. A., Zanotti, G., Hajdu, J. & Johnson, L. N. (1984) *Biochem. J.* **218,** 45–60.
58. Schinzel, R. & Drueckes, P. (1991) *FEBS Lett.* **286,** 125–128.
59. Barford, D., Flint, A. J. & Tonks, N. K. (1994) *Science* **263,** 1397–1404.
60. Zhang, L. & Lee, E. Y. (1997) *Biochemistry* **36,** 8209–8214.
61. Baumann, M. & Brand, K. (1988) *Cancer Res.* **48,** 7018–7021.
62. Gurney, M. E., Heinrich, S. P., Lee, M. R. & Yin, H. S. (1986) *Science* **234,** 566–574.
63. Nicholls, A., Sharp, K. A. & Honig, B. (1991) *Proteins* **11,** 281–296.
64. Kraulis, P. J. (1991) *J. Appl. Crystallogr.* **24,** 946–950.
65. Merritt, E. A. & Murphy, M. E. P. (1994) *Acta Crystallogr. D* **50,** 869–873.